Serial CT Findings of *Paragonimus* Infested Dogs and the Micro-CT Findings of the Worm Cysts

Chang Hyun Lee, MD[1,2]
Jung-Gi Im, MD[1]
Jin Mo Goo, MD[1]
Hyun Ju Lee, MD[1]
Sung-Tae Hong, MD[3]
Cheng Hua Shen, MD[3]
Doo Hyun Chung, MD[4]
Kyu Ri Son, MD[1]
Jung Min Chang, MD[1]
Hong Eo, MD[1]

Index terms:
Computed tomography (CT), technology
Lung, diseases
Parasites

Korean J Radiol 2007;8:372-381
Received November 28, 2006; accepted after revision January 17, 2007.

[1]Department of Radiology and the Institute of Radiation Medicine, Seoul National University College of Medicine, Seoul 110-744, Korea; [2]Seoul National University Hospital, Healthcare Gangnam Center, Seoul 135-984, Korea; [3]Department of Parasitology and Tropical Medicine, and the [4]Department of Pathology, Seoul National University Hospital, Seoul 110-744, Korea

Address reprint requests to:
Jung-Gi Im, MD, Department of Radiology, Seoul National University College of Medicine, 28, Yeongeon-dong, Jongno-gu, Seoul 110-744, Korea.
Tel. (822) 2072-3338
Fax. (822) 743-6385
e-mail: imjg@snu.ac.kr

Objective: To investigate the serial CT findings of *Paragonimus westermani* infected dogs and the microscopic structures of the worm cysts using Micro-CT.

Materials and Methods: This study was approved by the committee on animal research at our institution. Fifteen dogs infected with *P. westermani* underwent serial contrast-enhanced CT scans at pre-infection, after 10 days of infection, and monthly thereafter until six months for determining the radiologic-pathologic correlation. Three dogs (one dog each time) were sacrificed at 1, 3 and 6 months, respectively. After fixation of the lungs, both multi-detector CT and Micro-CT were performed for examining the worm cysts.

Results: The initial findings were pleural effusion and/or subpleural ground-glass opacities or linear opacities at day 10. At day 30, subpleural and peribronchial nodules appeared with hydropneumothorax and abdominal or chest wall air bubbles. Cavitary change and bronchial dilatation began to be seen on CT scan at day 30 and this was mostly seen together with mediastinal lymphadenopathy at day 60. Thereafter, subpleural ground-glass opacities and nodules with or without cavitary changes were persistently observed until day 180. After cavitary change of the nodules, the migratory features of the subpleural or peribronchial nodules were seen on all the serial CT scans. Micro-CT showed that the cyst wall contained dilated interconnected tubular structures, which had communications with the cavity and the adjacent distal bronchus.

Conclusion: The CT findings of paragonimiasis depend on the migratory stage of the worms. The worm cyst can have numerous interconnected tubular channels within its own wall and these channels have connections with the cavity and the adjacent distal bronchus.

Paragonimiasis is a food-borne disease, and it is caused by lung flukes *(Paragonimus)* of the genus *Paragonimus*. Among more than 45 species of lung flukes described from various parts of the world, only 12 of these species infect human (1). The most common and wide-spread species is *P. westermani*. Human cases of paragonimiasis have been reported mostly from Japan, Korea, Formosa, China, Manchuria, the Philippine Islands, India, parts of tropical West Africa and Latin America (2–15). An estimated 22 million people are infected worldwide with paragonimiasis (16).

The radiographic and computed tomographic (CT) findings of patients with pleuropulmonary paragonimiasis have been reported on by several authors (5, 17–19). The CT findings of pleuropulmonary paragonimiasis are known to be subpleural or subfissural nodules that contain low-attenuation areas, and these nodules are accompanied with pleural thickening and subpleural linear opacities (18). The

radiologic features of paragonimiasis can sometimes mimic pulmonary tuberculosis or lung cancer (15, 17, 18). Moreover, this type lesion also can be seen as high uptake on fluorodeoxyglucose-positron emission tomography (FDG-PET) (18, 20). Therefore, it is important to understand this disease's serial radiologic manifestations as they are correlated with the pathological progress.

After penetration into the lungs, the juvenile worms migrate until they settle down to form a cyst, which is the most consistent change noted in the lung parenchyma. Im et al. (17) performed an experimental study on 21 cats and they reported the high resolution CT findings after the lungs were harvested. However, that study was not an in vivo study showing the chronologically evolving changes in the same subjects. The nature of the morphological changes of this worm cyst in pulmonary paragonimiasis is still debatable (2, 21). There was a previous histopathologic study of the lungs infected with *P. westermani* in dogs, but it didn't report on the serial radiologic manifestations (22). The dog is a good definitive host of *P. westermani* and it undergoes the same pathological findings as do humans (22).

The purpose of this study was to investigate the serial CT findings in *Paragonimus* infected dogs and the relationship between the cavitary changes of the worm cysts and the adjacent bronchus using Micro-CT.

MATERIALS AND METHODS

The experimental protocols used in this study were approved by the committee on animal research at our institution. Fifteen dogs (12−16 months in age, 16−20 kg each, 10 males and 5 females) were infected with the metacercariae of *P. westermani* isolated from the muscles and gills of the freshwater crayfish, *Cambaroides similes*, by a parasitologist who had six years experience; the resultant cysts were followed up for six months using a multi-detector row (MDCT) scanner. CT scans were done before and 10 days after the infection, and then monthly follow-up CT scans were performed. Three dogs were randomly selected and one each was sacrificed at 1, 3 and 6 months, respectively, after the CT scans during the study period for determining the radiologic-pathologic correlation. After the experimental study, the other 12 dogs were necropsied at the Department of Parasitology and Tropical Medicine to recover the adult worms. The lungs were inflated and fixed by Heitzman's method. The CT scan images and contact radiographs of the pathologic specimens were then obtained.

Induction of Infection

The freshwater crayfish (*Cambaroides similis*) were acquired in JeollaNam-do, Korea. After metacercariae of *P. westermani* were isolated with using a stereomicroscope, they were introduced into the stomach of each dog (180−200 metacercariae in 10 dogs, 80 metacercariae in 5 dogs) through a gastric tube by a parasitologist. Anesthesia for CT scanning was induced with an intramuscular injection of 10 mg/kg of body weight ketamine hydrochloride (Ketalar®; Yuhan Yanghang, Seoul, Korea) and 4 mg/kg of xylazine hydrochloride (Rompun® 2%; Bayer Korea, Seoul, Korea); this anesthesia was maintained with intravenous injections of 10 mg/kg of zolazepam (Zoletil®; Virbac, Carros, France) by a specialist who had 10 years experience in laboratory animal care and research. The antecubital vein was catheterized with an 18-gauge plastic cannula for injecting the contrast material. The CT scans were acquired during quiet self-breathing of the dog.

Pathological Specimens

After the scheduled CT examinations, the three dogs were sacrificed with an intravenous injection of a lethal amount of thiopental sodium (Pentothal; Choongwae Pharm, Seoul, Korea). The autopsies were performed by an experienced parasitologist and they were observed by a radiologist. The lungs were investigated and any pathological finding in the thorax and upper abdomen were photographed. After fixation of the lungs, CT scans of the specimens were performed as described later and the specimens were then sliced to a thickness of 3−5 mm in the anatomical axial planes corresponding to those in which the CT images were obtained.

Each slice was carefully examined and contact radiographs (Faxitron 43805N; Hewlett-Packard, Sunnyvale, CA and X-Omat V; Eastman Kodak, Rochester, NY) were obtained of the representative slices that contained consolidation, bronchial dilatation and worm cysts. Representative areas of the pathological samples for slide preparation were selected by two radiologists working in consensus. After the locations of the sampled areas had been recorded, the selected tissues were prepared for fixation, paraffin embedding, cutting and then staining with hematoxylin-eosin in the usual manner.

CT and Micro-CT Protocol

The 4-row multidetector CT (MX 8000, Philips Medical Systems, Cleveland, OH) scan was performed with the dogs in the supine position and using the following scanning parameters: 120 kVp, 150 mA, 0.75 second per rotation, 3.2/1.6-mm reconstruction thickness/increment, 3.2-mm section thickness and 12.5/1.25 table speed (mm

per rotation)/pitch. After injection of 2.5 mL/kg of contrast material (Iopromide, Ultravist 370; Schering, Berlin, Germany) at a rate of 2 mL/sec, scanning was started at 25 second after contrast injection from the apex of the lungs to the level of the lower pole of the kidneys.

For the fixed lung specimens, 16-row multidetector CT (Sensation 16; Siemens Medical Systems, Erlangen, Germany) scanning was performed with using the following scanning parameters to acquire more thin section CT images: 120 kVp, 150 mA, 0.5 second per rotation, 0.75 – mm reconstruction thickness, 0.75-mm section thickness and 5.4/12-mm table speed (mm per rotation)/pitch; Micro-CT (Skyscan 1076; Skyscan, Aartselaar, Belgium) scanning was performed using the following scanning parameters: source voltage = 40 kVp, source current = 200 uAm, camera pixel size = 11.7 um, image pixel size = 35.2 um, rotation step = 0.3 degree, frame averaging = 2, scanning position = 58.0 mm and section thickness = 18 um. The Micro-CT scan data was reconstructed into 3D images for evaluating the worm cysts and their relation to airways (Amira 4.0; Mercury Computer Systems, Berlin, Germany).

Image Analysis

CT images were evaluated in terms of (a) subpleural ground-glass opacity (b) subpleural linear opacity (c) subpleural and peribronchial rim enhancing nodules (d) cavitary change of the nodules (e) bronchial dilatation (f) pleural effusion (g) pneumothorax (h) air bubbles in the abdominal or chest wall, and (i) migratory features of the

Table 1. Serial CT Findings of *Paragonimus* Infected Dogs

CT Findings (%)	10 days (n = 15)	30 days (n = 15)	60 days (n = 14)	90 days (n = 14)	120 days (n = 13)	150 days (n = 13)	180 days (n = 13)
Subpleural GGO	20 (3)	100 (15)	100 (14)	100 (14)	100 (13)	100 (13)	100 (13)
Subpleural linear opacities	20 (3)	47 (7)	50 (7)	43 (6)	46 (6)	38 (5)	31 (4)
Subpleural rim-enhancing nodules	7 (1)	100 (15)	100 (14)	100 (14)	100 (13)	100 (13)	100 (13)
Peribronchial rim-enhancing nodules	7 (1)	100 (15)	100 (14)	100 (14)	100 (13)	100 (13)	100 (13)
Bronchial dilatation	0 (0)	0 (0)	50 (7)	50 (7)	31 (4)	31 (4)	23 (3)
Cavitary change	0 (0)	7 (1)	86 (12)	100 (14)	100 (13)	100 (13)	100 (13)
Lymph node enlargement	0 (0)	13 (2)	64 (9)	100 (14)	100 (13)	100 (13)	100 (13)
Pleural effusion	27 (4)	73 (11)	71 (10)	64 (9)	77 (10)	77 (10)	77 (10)
Pneumothorax	0 (0)	93 (14)	93 (13)	64 (9)	85 (11)	92 (12)	77 (10)
Abdominal or chest wall air bubble	0 (0)	93 (14)	93 (13)	64 (9)	62 (8)	62 (8)	62 (8)

Note.—GGO = ground-glass opacity, Data in parentheses are the numbers of dogs (each one of the three dogs was harvested at 1, 3 and 6 months after CT scans).

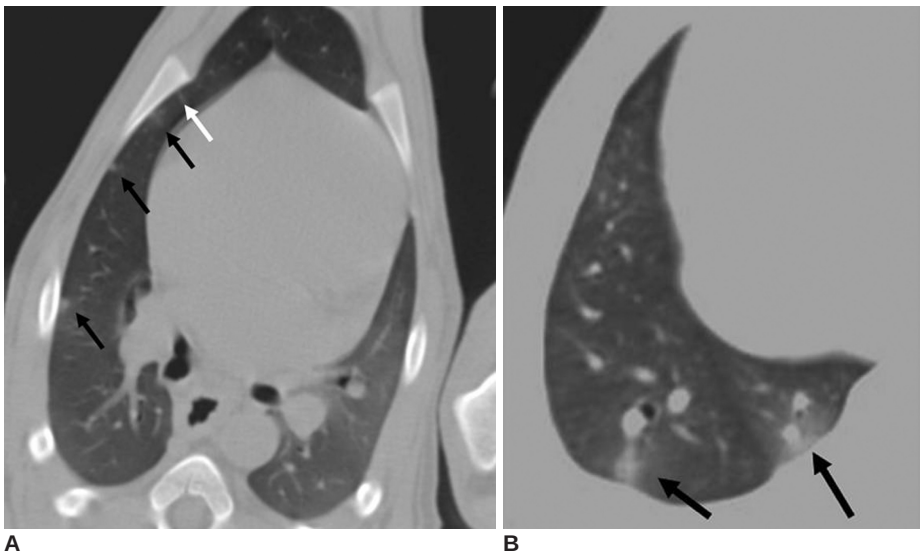

A **B**

Fig. 1. A, B. CT findings of the dogs 10 days after *P. westermani* metacercariae infusion into the stomach. A subpleural line (white arrow in **A**), subpleural nodules (black arrows in **A**) and nodules with or without ground-glass opacity (black arrows in **B**) are seen.

nodules and/or the worm cysts (17–19). Two experienced chest radiologists, who were aware of the time since infection and the number of infused metacercariae, reviewed all the CT scans and Micro-CT images after six months. An experienced lung pathologist together with a parasitologist and two radiologists assessed the histopathological specimens for findings that might correspond to and help explain the CT findings.

Statistical Analysis

Statistical analysis was performed with GraphPad InStat, version 3.05, software (GraphPad, San Diego, CA, www.graphpad.com). McNemar's test was used to compare the incidences of pneumothorax, abdominal and

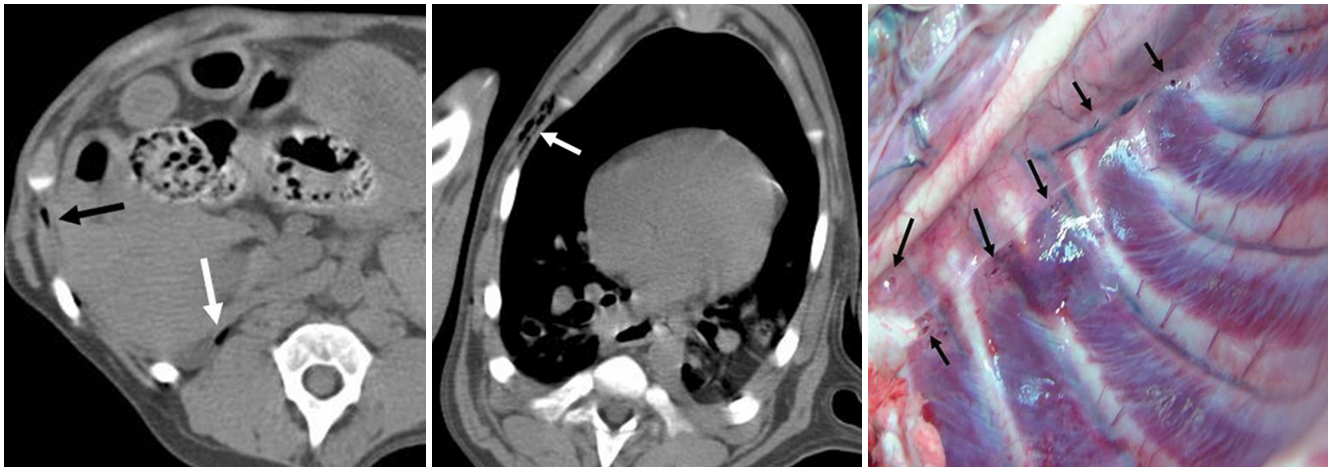

Fig. 2. CT findings and a photograph obtained at autopsy (**C**) of dogs at 30 days after *P. westermani* metacercariae infusion into the stomach.
A. Air bubbles in the intercostal muscles (black arrow) and retrocrural space (white arrow) in the upper abdomen.
B. Air bubbles in the intercostal muscles and subcutaneous tissue (white arrow) in the chest wall.
C. Multiple holes (black arrows) in the parietal pleura of the chest wall (×1).

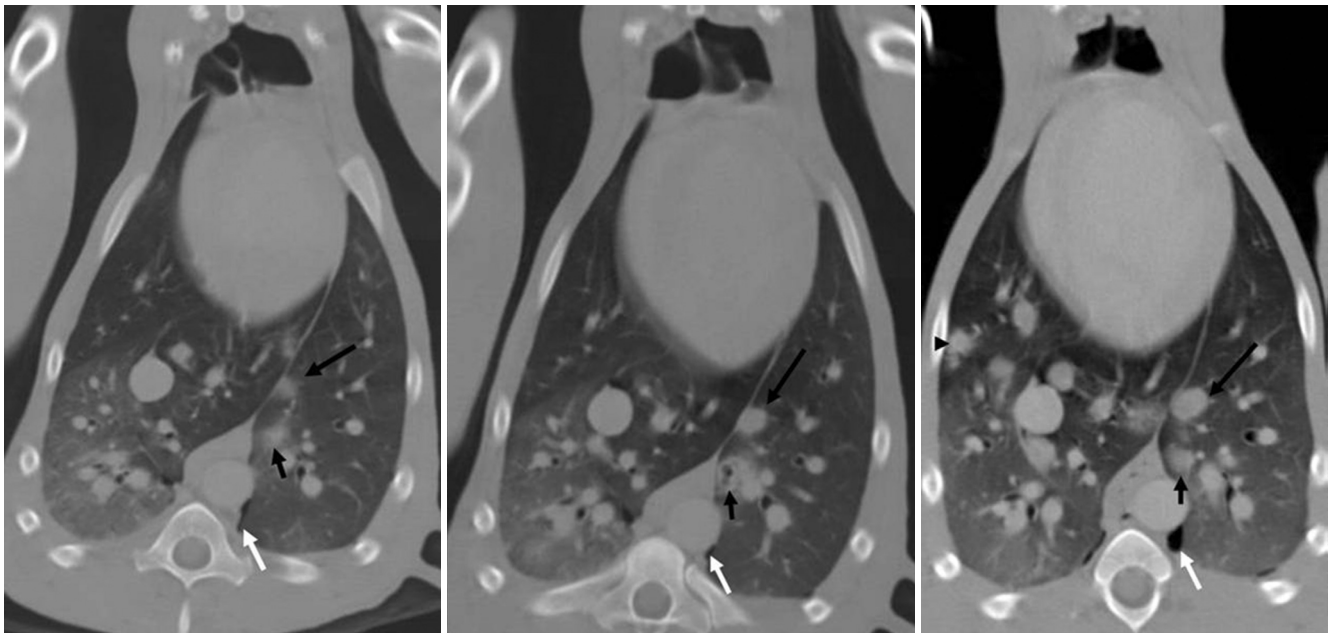

Fig. 3. Serial CT findings of a dog infected with *P. westermani*.
A. At 30 days, subpleural (long black arrow) and peribronchial nodules (short black arrows in **A**–**C**) are seen. A small amount of pneumothorax (white arrows in **A**–**C**) is also seen.
B. At 60 days, the size of the subpleural nodule is increased and the peribronchial nodules show cavitary change.
C. At 90 days, the size of the subpleural nodule is increased. The cavitary change disappeared in the peribronchial nodule. Note the newly appeared nodule in the right lung (arrowhead).

chest wall air-bubbles and pleural effusion at 30 days and 90 days, respectively. A p value of 0.05 was considered to indicate a statistically significant difference.

RESULTS

Serial CT Findings

The sequential CT findings are summarized in Table 1. The findings observed at the early stage of disease were pleural effusion (27%, 4/15), and/or subpleural nodular lesion with or without ground-glass opacities and linear opacities at day 10 (Fig. 1). At day 30, subpleural or peribronchial nodules appeared with an increased rate of the pleural effusion (73%, 11/15), pneumothorax (93%, 14/15), and abdominal or chest wall air bubbles (93%, 14/15) (Fig. 2). Pneumoperitoneum was not seen in any of the cases. Cavitary changes of the nodules started to be seen on the CT scan at day 30 (7%, 1/15) and mostly at day 60 (86%, 12/14) (Fig. 3). Bronchial dilatation was seen after day 60. Most nodules were seen with peripheral ground-glass opacities and some showed rim enhancement along the capsular wall with internal low density on the contrast-enhanced CT scan (Fig. 4). Subpleural ground-glass opacities and subpleural nodules with or without cavitary changes were consistently demonstrated untill termination of the experiment at day 180, and after they were seen on CT scans. After the cavitary changes of the nodules, the migratory features of the subpleural or peribronchial nodules were seen on all the serial CT scans (Fig. 5). The mediastinal lymph nodes were also enlarged after 60 days and this mostly occurred in the subcarinal and left paratracheal regions (Fig. 4). The incidence of

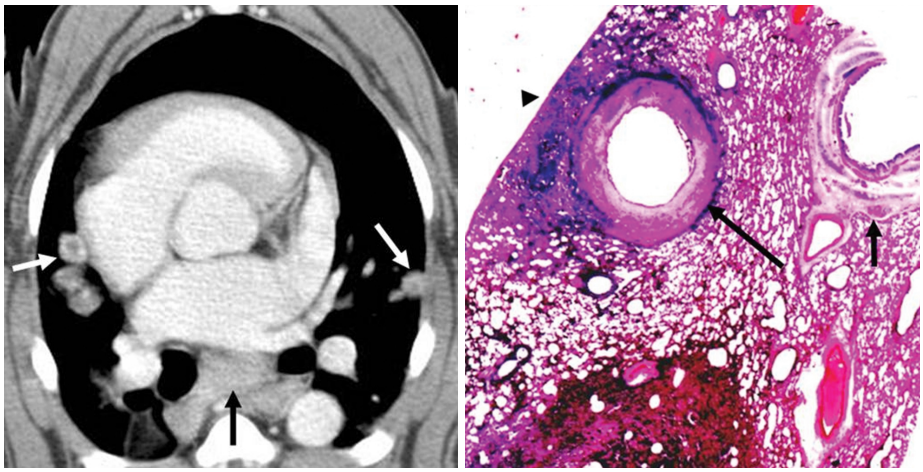

Fig. 4. Contrast-enhanced CT and photomicrographic findings of a dog at 90 days after being infected with *P. westermani*.
A. Contrast-enhanced CT shows rim enhancing subpleural nodules with internal low attenuation (white arrows) in both lungs. Subcarinal lymphadenopathy is also seen (black arrow).
B. Photomicrograph of the worm cyst shows the capsular rim (long black arrow) and adjacent bronchus (short black arrow) (Hematoxylin & Eosin staining, ×1). Note the subpleural location of the worm cyst and the inflammatory changes from the pleural surface to the cyst (arrowhead).

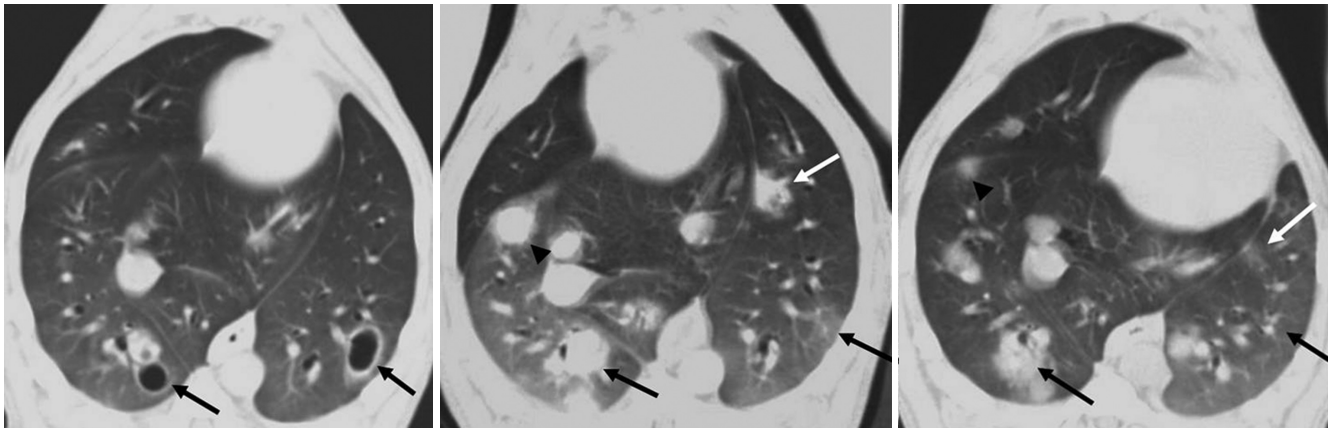

Fig. 5. Serial CT findings of nodules in a dog infected with *P. westermani*.
A. Two well defined thin-walled cystic lesions (black arrows) are seen in both lower lobes at 90 days.
B. The cystic lesions have disappeared (black arrows) and other subpleural nodules have developed (white arrow, black arrowhead) at 120 days.
C. The left subpleural nodule (white arrow) has nearly disappeared and the right subpleural nodule (black arrowhead) has decreased in size at 150 days. Also note slight change in nodule size in both lower lobes (black arrows).

pneumothorax and air bubbles in the abdominal or chest walls was significantly decreased at day 90 (p = 0.02, odd ratio = 0.11, 95% CI: 0.003–0.802). The incidence of pleural effusion also slightly decreased, but this was not statistically significant (p = 0.26, odd ratio = 0.44, 95% CI: 0.1–1.5) at day 90.

We could observe increased numbers (mean number: 25.3 versus 11.5, respectively) of nodules or cysts and a prolonged duration (mean time: 5 months versus 1.7 months, respectively) of the hydropneumothorax in the cases of heavy infection versus cases of light infection. However, there was no difference in the chronologic CT findings between the numbers of infused metacercariae (80 in 5 dogs versus 180–200 in 10 dogs).

Specimen Radiographs and MDCT Scans of the Fixed Lungs

The sliced sections of the fixed lungs at one month showed subpleural consolidation or ground-glass opacity that was headed toward the central airways (Fig. 6). This pathologically corresponded to the hemorrhagic consolidations noted in all the specimens (Fig. 7). The CT scans of the fixed lungs showed some cystic lesions with internal crescentic structures that were not demonstrated on the in vivo CT scans. These internal structures were the adult worms inside the cysts (Fig. 7). The other findings that were observed on the CT scans of the fixed lungs were the same as those seen on the in vivo CT scans (Table 1).

Micro-CT Findings of the Worm Cysts

On Micro-CT, the worm cysts appeared as a cyst that typically contained two worms. Some cysts, however, did

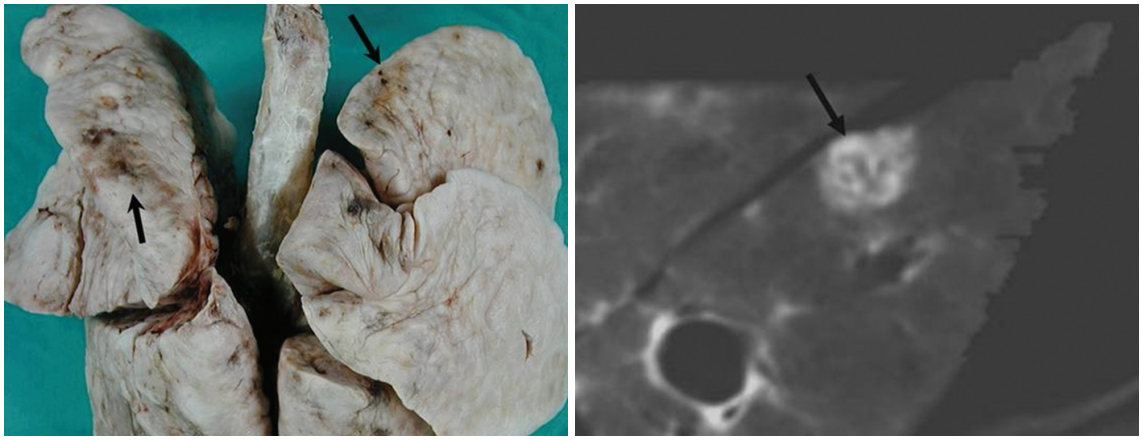

A **B**

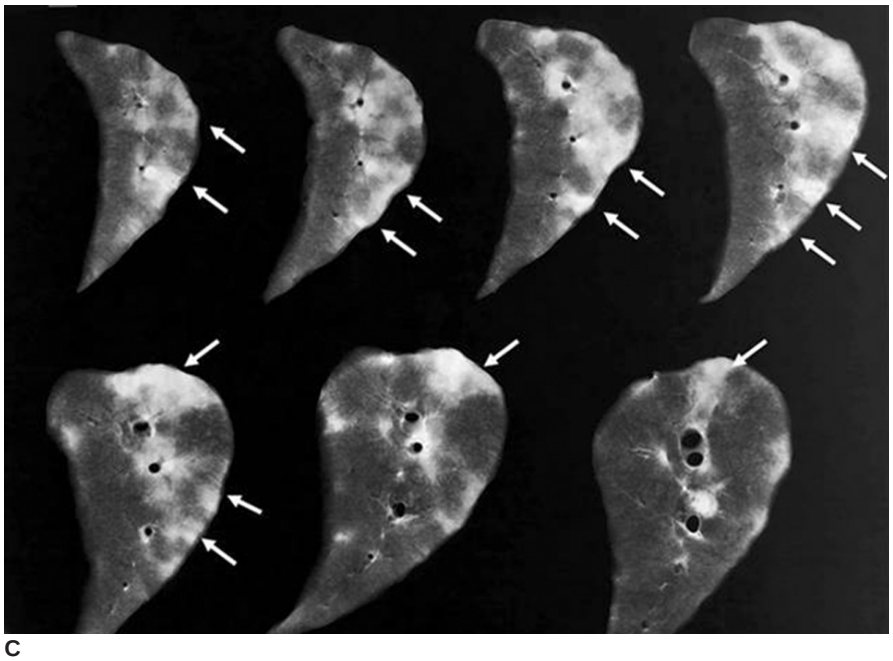

C

Fig. 6. Photograph and CT scan, for the fixed lungs prepared with Heitzman's method, of a dog after being infected for 30 days with *P. westermani*.
A. Photograph of the fixed lung shows multiple pleural spots with areas of hemorrhages (black arrows).
B. CT scan of the fixed lung shows a subpleural nodule with bronchioloectasis (black arrow).
C. Consecutive contact radiographs show subpleural opacities (white arrows) directed toward the central airways.

not have the accompanying worms. These were presumed to be lost during the preparation or to migration. The cyst wall had many dilated interconnecting channels connected to the distal airways, which were not clearly identified on the CT scans (Fig. 8). The cysts were located adjacent to the airways and some had linear tracks from the pleura. We could not observe respiratory epithelium, but inflammatory cells and fibrosis were observed in the wall of the cysts. The nodular opacities around the cyst were eggs and granulomas in the pathologic specimens. The reconstructed three-dimensional images of the specimens after fixation showed that mature worms resided within the cyst (Fig. 8) and this corresponded to the microphotographs. There was no difference of the Micro-CT findings of the worm cysts that were obtained at 1, 3 and 6 months, respectively.

DISCUSSION

We demonstrated the chronologically ordered serial CT findings of untreated Paragonimus infected dogs. The serial CT scans uniformly showed the characteristic migrating features, depending on the migratory stage of the worms.

The life cycle of these flukes involves two intermediate hosts and also definitive hosts, including humans. The adult flukes live in the lungs of human or carnivorous mammals, and these adults deposit eggs into the bronchi. The eggs are expelled either by coughing or through the feces after they are swallowed. The eggs then develop in water for 2–3

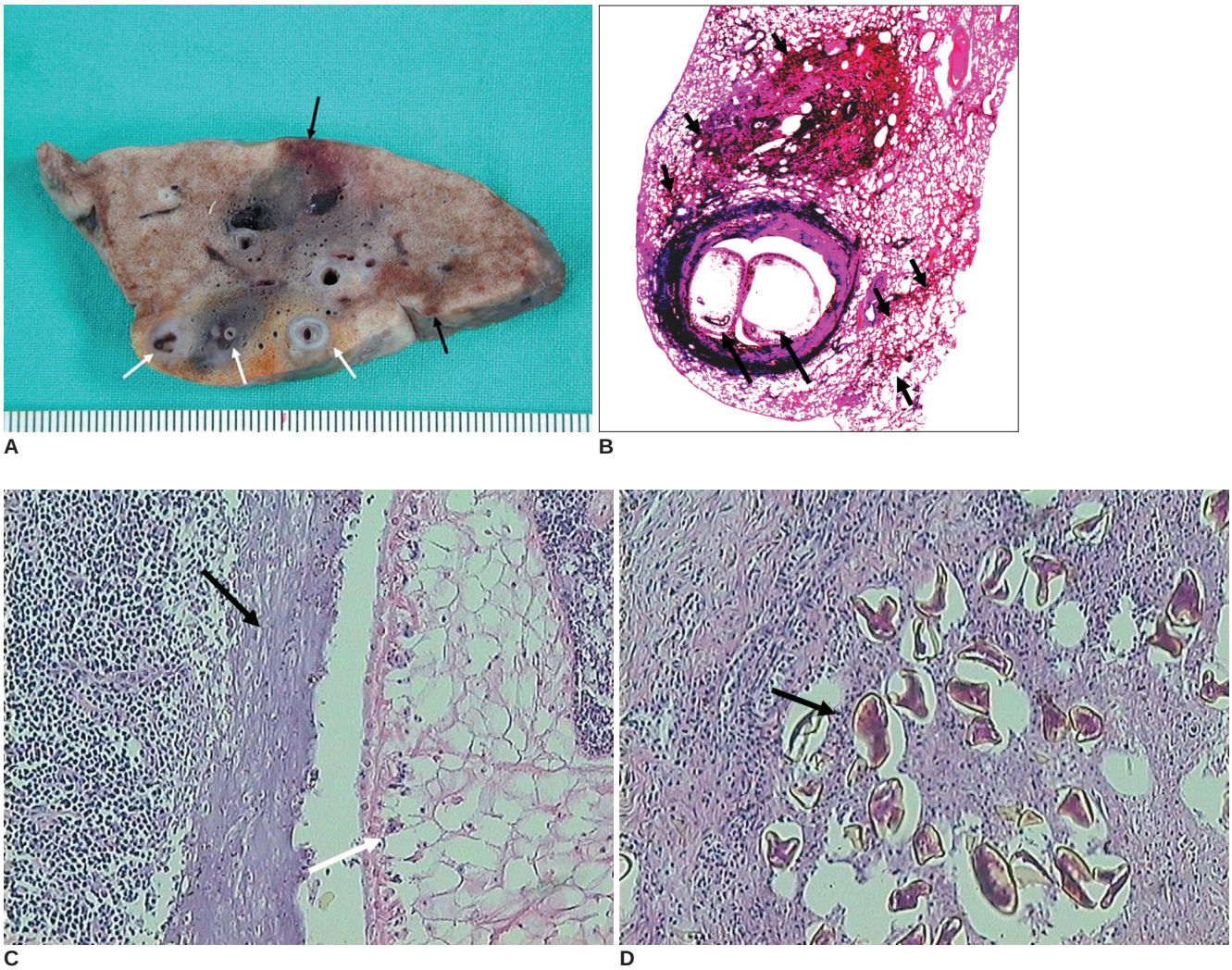

Fig. 7. The formalin-fixed lung harvested from a dog at 90 days.
A. The sliced lung segment shows subpleural hemorrhagic consolidations (black arrows) and juvenile worms growing inside the cystic lesions or dilated bronchioles (white arrows).
B. Photomicrograph of the worm cyst shows two adult worms inside the cyst (long arrows). There are hemorrhages (short arrows) around the cyst and dilated distal airways. (Hematoxylin & Eosin staining, ×1)
C. The wall of the cyst consists of fibrous tissue and inflammatory cells (black arrow). An adult worm (white arrow) is seen inside the cyst. (Hematoxylin & Eosin staining, ×100)
D. Note the eggs in the alveoli (black arrow), which are produced by adult worms. (Hematoxylin & Eosin staining, ×100)

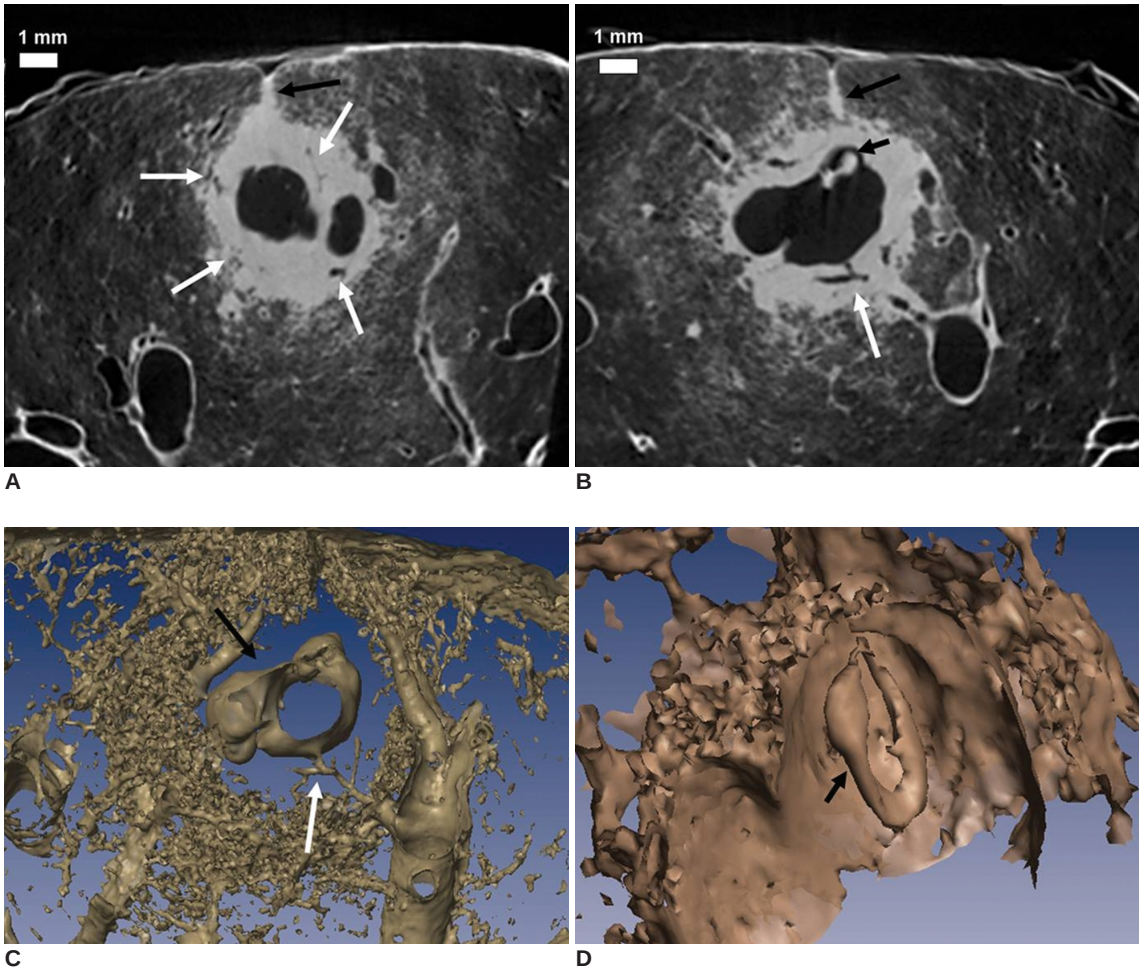

Fig. 8. Micro-CT findings of the worm cyst in the formalin-fixed lung harvested from a dog at 180 days. The chocolate colored fluid within the worm cyst was evacuated during the fixation and drying procedure. The white bar in the left upper corner indicates 1 mm.
A. Micro-CT scan shows a subpleural worm cyst with a subpleural track (long black arrows in **A, B**). Dilated distal airways (white arrows) are shown within the wall or capsule of the cyst.
B. A connection between the worm cyst and the distal airways is seen (white arrow) and note the adult worm inside the cyst (short black arrow).
C, D. 3D reconstruction image of the Micro-CT scans shows a connection between the worm cyst (black arrow) and the distal airway (white arrow) and the worm cyst contains an adult worm (short black arrow in **D**).

weeks and they ultimately release miracidia; these invade the first intermediate snail host, *Semisulcospira* species. The miracidia develop through sporocysts, redia and cercariae in the snail, and the cercariae then emerge and invade the second intermediate host. Freshwater crustacean such as crabs or crayfish are the second intermediate hosts, in which the cercariae become metacercariae. Humans eat pickled freshwater crab in endemic areas; when humans ingest the infected crustaceans, the metacercariae excyst into the small intestine; the juvenile flukes develop and penetrate the intestinal wall into the peritoneal cavity (2). They then migrate into the abdominal wall or liver, where they undergo further development. Approximately one week later, the adult flukes reenter from the abdominal cavity and penetrate the diaphragm to reach the pleural space and lungs (2).

The lung fluke (its size is about $7-12 \times 4-7$ mm) is rather plump and egg-shaped and it is oval on the transverse section (2). Usually, the adult worms are not easily depicted on in vivo CT scanning because there is accompanying chocolate color fluid inside the cyst. When they have a connection with the distal airways, the fluid or secretions from the worms can be evacuated from the nodular lesion; the adult worms are usually seen as concave structures on CT scan only before they migrate to a different location. The worm cyst is seen as a nodule showing internal low attenuation and rim enhancement on contrast enhanced CT scan in humans (18).

The juvenile worms travel through the diaphragm to get to the pleural cavity from the peritoneal cavity (2).

Yokogawa (2) investigated the migratory route of juvenile *P. westermani* in cats and rats. They found that the juvenile worms migrating into the abdominal cavity immediately entered the inner wall of the abdominal cavity. Several cases of early stage paragonimiasis have been reported; the authors described that they present as a subcutaneous induration or mass in the abdominal subcutaneous tissue (23–25). We observed subcutaneous air bubbles at day 30 in the subcutaneous tissues of the abdominal wall or chest wall on CT, and this has not been reported previously. This finding was demonstrated when hydropneumothorax started to be seen. We can speculate that the air bubbles are the radiologic evidence of its migration route through the abdominal and chest wall to the pleural cavity. In our study, we infused a relatively large number of metacercariae compared to the previous experimental studies (17, 22). This heavy infection might have helped us to observe the air bubbles in the abdominal or chest wall. We could not find any case of pneumoperitoneum that occurred during paragonimiasis in the literature. Pneumoperitoneum was also not demonstrated in this study, and this may be related to the duration of stay of the metacercariae in the abdominal cavity after penetration of the small intestine and mesenteries covering the bowels.

The incidence of pneumothorax decreased from 93% to 64% at day 90. Im et al. (17), in the experimental study of cats, reported that the rate of pneumothorax decreased at 12 weeks. The initially infected juvenile worms grow into adult worms and they then spill eggs within the worm cyst in the lung parenchyma and next they migrate toward the proximal bronchus. Therefore, the decreased incidence of pneumothorax at day 90 might be explained by the maturation of the worm cysts. After forming the worm cysts, the worms migrate less actively than they did during the early stage of infection in the lungs.

The prevalence of pleural effusion in patients with pulmonary paragonimiasis varies from 3% to 54% (5, 12, 17). In our experimental study, pleural effusion was initially noted at day 10 (27%, 4/15) and the incidence increased at day 30 (73%, 11/15). Yokogawa (2), in his experimental study of cats, also reported that the juvenile worms appear in the pleural cavity after penetrating the diaphragm about 14 days after infection. The recently reported articles showed a little lower rate of the pleural effusion or pneumothorax compared to the older previous reports (7, 18, 19). This might be related to the differences in the stage of disease when the patients visited a hospital, the smaller number of metacercariae ingested and the earlier diagnosis, which was based on antibody testing done during the early stage of active worm migration (17).

Im et al. (5, 17) reported that when the worm cyst has a connection with the bronchus, then air or gas appears within the cyst on CT. In this study with using Micro-CT, we demonstrated that the cyst wall has dilated tubular structures connected with each other. This microstructure of the worm cyst illustrates the ways how eggs generated from adult worms can spread to the lung parenchyma and the distal airways through the wall, which functions as a pathway for the worms or eggs to move through. Three-dimensional reconstruction of the Micro-CT images helped us reveal the shape of the cyst and we tried to avoid loss of the worms inside the worm cyst during the slicing and preparations to make the histopathological slides.

The limitation of this study is that this level of heavy infection does not usually occur in humans. The CT findings of human paragonimiasis generally show a single nodular or cavitary lesion; however, the chronologic CT findings of paragonimiasis in humans have not yet been demonstrated (18). In our study, although the amount of profusion of the lung lesions and the duration and amount of pneumothorax appear to decrease in the cases of light infection, the chronologic CT findings were not different. So, we feel that the results of our experimental study may be applied to paragonimiasis in humans if we give consideration to the degree of infection. The chronologic CT findings of the worm cysts may explain the migration of the adult worms, which stay in the worm cyst after the cavitary change of the subpleural or peribronchial nodules, even in humans.

A single nodular or cavitary lesion seen on humans can mimic pulmonary tuberculosis or lung cancer, and these lesions can show an increased FDG-PET uptake (18, 20). Moreover, most of the recent reported cases in clinical practice were initially suspected to be lung cancer or tuberculosis (7). Therefore, it is important for the radiologist to understand the various CT findings of pulmonary paragonimiasis according to their migration so as to avoid unnecessary invasive procedures.

In conclusion, the CT findings of pulmonary paragonimiasis depend on the migratory stage of the worms. The worm cyst can have numerous interconnected tubular channels within its own wall and these channels have connections with the cyst cavity and the adjacent distal bronchus.

References

1. Sachs R, Albiez EJ, Voelker J. Prevalence of Paragonimus uterobilateralis infection in children in a Liberian village. *Trans R Soc Trop Med Hyg* 1986;80:800-801
2. Yokogawa M. Paragonimus and paragonimiasis. *Adv Parasitol* 1969;7:375-387
3. Sadun EH, Buck AA. Paragonimiasis in South Korea:

immunodiagnostic, epidemiologic, clinical, roentgenologic and therapeutic studies. *Am J Trop Med Hyg* 1960;9:562-599
4. Choi DW. Paragonimus and paragonimiasis in Korea. *Korean J Parasitol* 1990;28(Suppl):79-102
5. Im JG, Whang HY, Kim WS, Han MC, Shim YS, Cho SY. Pleuropulmonary paragonimiasis: radiologic findings in 71 patients. *AJR Am J Roentgenol* 1992;159:39-43
6. Shim YS, Cho SY, Han YC. Pulmonary paragonimiasis: a Korean perspective. *Semin Respir Med* 1991;12:35-45
7. Jeon K, Koh WJ, Kim H, Kwon OJ, Kim TS, Lee KS, et al. Clinical features of recently diagnosed pulmonary paragonimiasis in Korea. *Chest* 2005;128:1423-1430
8. Roque FT, Ludwick RW, Bell JC. Pulmonary paragonimiasis; a review with case reports from Korea and the Philippines. *Ann Intern Med* 1953;38:1206-1221
9. Suwanik R, Harinsuta C. Pulmonary paragonimiasis; an evaluation of roentgen findings in 38 positive sputum patients in an endemic area in Thailand. *Am J Roentgenol Radium Ther Nucl Med* 1959;81:236-244
10. Vélez I, Vélasquez LE, Vélez ID. Morphological description and life cycle of Paragonimus sp. (Trematoda: Troglotrematidae): causal agent of human paragonimiasis in Colombia. *J Parasitol* 2003;89:749-755
11. Nwokolo C. Outbreak of paragonimiasis in Eastern Nigeria. *Lancet* 1972;1:32-33
12. Johnson RJ, Johnson JR. Paragonimiasis in Indochinese refugees. Roentgenographic findings with clinical correlations. *Am Rev Respir Dis* 1983;128:534-538
13. Johnson JR, Falk A, Iber C, Davies S. Paragonimiasis in the United States. A report of nine cases in Hmong immigrants. *Chest* 1982;82:168-171
14. Burton K, Yogev R, London N, Boyer K, Shulman ST. Pulmonary paragonimiasis in Laotian refugee children. *Pediatrics* 1982;70:246-248
15. Collins MS, Phelan A, Kim TC, Pearson RD. Paragonimus westermani: a cause of cavitary lung disease in an Indochinese refugee. *South Med J* 1981;74:1418-1420
16. World Health Organization (WHO). Report of Joint WHO/FAO workshop on foodborne trematode infections in Asia. 2004;40-41
17. Im JG, Kong Y, Shin YM, Yang SO, Song JG, Han MC, et al. Pulmonary paragonimiasis: clinical and experimental studies. *Radiographics* 1993;13:575-586
18. Kim TS, Han J, Shim SS, Jeon K, Koh WJ, Lee I, et al. Pleuropulmonary paragonimiasis: CT findings in 31 patients. *AJR Am J Roentgenol* 2005;185:616-621
19. Kuroki M, Hatabu H, Nakata H, Hashiguchi N, Shimizu T, Uchino N, et al. High-resolution computed tomography findings of P. westermani. *J Thorac Imaging* 2005;20:210-213
20. Watanabe S, Nakamura Y, Kariatsumari K, Nagata T, Sakata R, Zinnouchi S, et al. Pulmonary paragonimiasis mimicking lung cancer on FDG-PET imaging. *Anticancer Res* 2003;23:3437-3440
21. Diaconita GH, Goldis GH. Investigations on pathomorphology and pathogenesis of pulmonary paragonimiasis. *Acta Tuberc Scand* 1964;44:53-75
22. Lee OR. A histopathologic study of the lungs infected with Paragonimus westermani in the dog. *Korean J Parasitol* 1979;17:19-44 (Korean)
23. Mizuki M, Mitoh K, Miyazaki E, Tsuda T. A case of Paragonimiasis westermani with pleural effusion eight months after migrating subcutaneous induration of the abdominal wall. *Nihon Kyobu Shikkan Gakkai Zasshi* 1992;30:1125-1130
24. Choi WY, Jeong SS. A case of paragonimiasis in the abdominal subcutaneous tissue. *Korean J Parasitol* 1991;29:407-409
25. Takemasa H, Saito K, Nakayamada S, Kanazawa T, Tanaka Y. A case of Paragonimiasis westermani complicated with migrating subcutaneous induration and multiple involvements in the liver. *Kansenshogaku Zasshi* 2002;76:594-599